

LETTER TO THE EDITOR

The *Herschel*[★] view of star formation in the Rosette molecular cloud under the influence of NGC 2244^{★★}

N. Schneider¹, F. Motte¹, S. Bontemps^{1,2}, M. Hennemann¹, J. Di Francesco³, Ph. André¹, A. Zavagno⁴, T. Csengeri¹, A. Men'shchikov¹, A. Abergel⁵, J.-P. Baluteau⁴, J.-Ph. Bernard⁶, P. Cox⁷, P. Didelon¹, A.-M. di Giorgio⁸, R. Gastaud¹, M. Griffin⁹, P. Hargrave⁹, T. Hill¹, M. Huang¹⁰, J. Kirk⁹, V. Könyves¹, S. Leeks¹¹, J. Z. Li¹⁰, A. Marston¹², P. Martin¹³, V. Minier¹, S. Molinari⁸, G. Olofsson¹⁴, P. Panuzzo¹, P. Persi¹⁵, S. Pezzuto⁸, H. Roussel¹⁶, D. Russeil⁴, S. Sadavoy³, P. Saraceno⁸, M. Sauvage¹, B. Sibthorpe¹⁷, L. Spinoglio⁸, L. Testi¹⁸, D. Teyssier¹², R. Vavrek¹², D. Ward-Thompson⁹, G. White^{11,21}, C. D. Wilson¹⁹, and A. Woodcraft²⁰

(Affiliations are available in the online edition)

Received 31 March 2010 / Accepted 6 May 2010

ABSTRACT

Context. The Rosette molecular cloud is promoted as the archetype of a triggered star-formation site. This is mainly due to its morphology, because the central OB cluster NGC 2244 has blown a circular-shaped cavity into the cloud and the expanding H II-region now interacts with the cloud.

Aims. Studying the spatial distribution of the different evolutionary states of all star-forming sites in Rosette and investigating possible gradients of the dust temperature will help to test the “triggered star-formation” scenario in Rosette.

Methods. We use continuum data obtained with the PACS (70 and 160 μm) and SPIRE instruments (250, 350, 500 μm) of the *Herschel* telescope during the science demonstration phase of HOBYS.

Results. Three-color images of Rosette impressively show how the molecular gas is heated by the radiative impact of the NGC 2244 cluster. A clear negative temperature gradient and a positive density gradient (running from the H II-region/molecular cloud interface into the cloud) are detected. Studying the spatial distribution of the most massive dense cores (size scale 0.05 to 0.3 pc), we find an age-sequence (from more evolved to younger) with increasing distance to the cluster NGC 2244. No clear gradient is found for the clump (size-scale up to 1 pc) distribution.

Conclusions. The existence of temperature and density gradients and the observed age-sequence imply that star formation in Rosette may indeed be influenced by the radiative impact of the central NGC 2244 cluster. A more complete overview of the prestellar and protostellar population in Rosette is required to obtain a firmer result.

Key words. ISM: clouds – dust, extinction – ISM: general – infrared: ISM – submillimeter: ISM

1. Introduction

The Rosette is a spectacular region due to its well-known emission nebula, powered by the central OB cluster NGC 2244 (Figs. 1, 2) that has blown a cavity into the molecular cloud. The expanding H II-region is interacting with a high-mass (few times $10^5 M_{\odot}$) star-forming molecular cloud at 1.6 kpc from the Sun (Williams et al. 1994; Schneider et al. 1998a; Heyer et al. 2006), creating photon dominated regions (PDRs) along the interface (Schneider et al. 1998b). Bright PAH emission, first seen in the IRAS bands by Cox et al. (1990), indicates the presence of warm dust. Near- and mid-IR surveys (Phelps & Lada 1997; Li & Smith 2005; Balog et al. 2007; Roman-Zuniga et al. 2008; Poulton et al. 2008) investigated the IR-population of Rosette in greater detail.

Ionizing radiation has an effect on the evolution of a molecular cloud and is thus closely linked with star formation.

Photoevaporation of gas on an existing (primordial) clumpy cloud structure causes the formation of *globules*. Well-known features in the Rosette molecular cloud (hereafter RMC) are the “elephant trunks”, “speck”- and “teardrop” globules (Schneps et al. 1980; White et al. 1997), which show bright rim emission. These globules can form low-mass stars and shrink slowly (e.g. Lefloch & Lazareff 1994). Rayleigh-Taylor instabilities can explain the elephant trunk globules in Rosette (e.g. Patel et al. 1993). Schneider et al. (1998a) showed that basically all CO clumps close to the H II-region collapse and form stars. Recently, Gritschneider et al. (2009) ran hydrodynamic models including turbulence and ionizing radiation. They showed that it is due to the heating and consequently the increasing pressure of the lower-density interclump gas that primordial, denser clumps are even more compressed, forming pillar-like structures that point towards the source of radiation. In the high-density ($n \sim 10^7 \text{ cm}^{-3}$) tip of the pillars, star formation takes place. However, the extent to which star formation is promoted deeper within the cloud, where the level of ionization is drastically falling, is not clear.

Although there is a clear influence of radiation on the evolution of the RMC in general, it is less clear what its specific

[★] *Herschel* is an ESA space observatory with science instruments provided by European-led Principal Investigator consortia and with important participation from NASA.

^{★★} Figures 5 and 6 are only available in electronic form at <http://www.aanda.org>

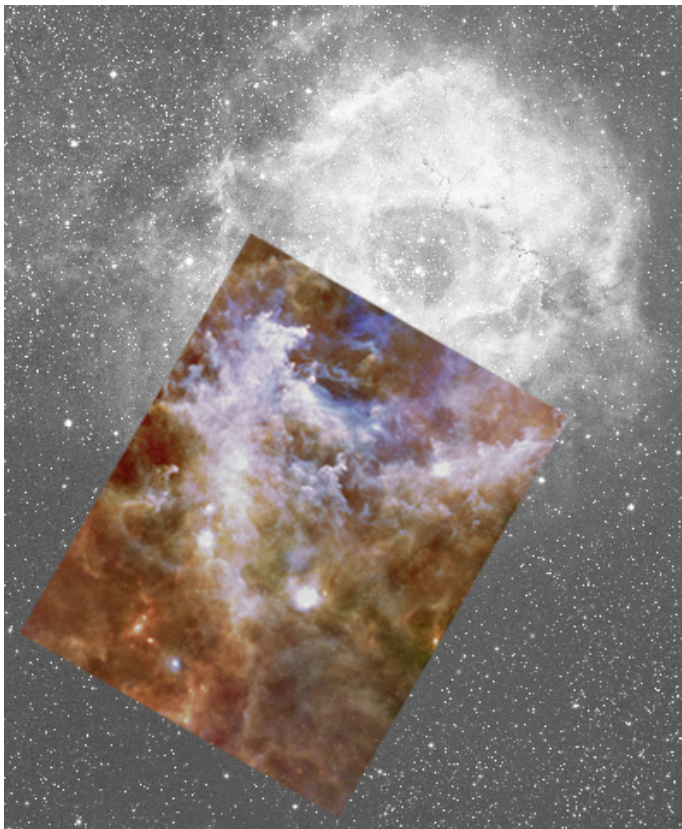


Fig. 1. Three-color image ($70\ \mu\text{m}$ = blue, $160\ \mu\text{m}$ = green, $500\ \mu\text{m}$ = red) of Rosette, overlaid on an optical image ($H\alpha$ from the Digital Sky Survey).

link to star formation is. In the classical picture of *sequential triggered* star formation (Elmegreen & Lada 1977), an expanding $H\text{II}$ -region assembles gas in the layer compressed between the ionization front and the shock front, which then fragments into gravitationally unstable dense cores that form stars. The ionization front of this new association propagates further into the cloud and induces the next generation of star formation.

The Rosette was proposed as an archetype of a triggered star formation site. Many other studies (e.g. Deharveng et al. 2005) have revealed possible candidates on smaller size scales with a clearly-defined, simple geometry and indications of star-formation in a swept-up shell of gas around a central $H\text{II}$ -region. The Rosette is a more demanding region, because it is a massive molecular cloud with a complex structure caused by the presence of at least three clusters that illuminate the $H\text{II}$ -region (NGC 2244, NGC 2237), and the recently detected RMC-XA (Wang et al. 2009). There are arguments that star-formation in Rosette may be the result of a triggering process:

- (i) Balog et al. (2007) and Roman-Zuniga et al. (2008) found that the average NIR excess fraction for stellar clusters *increases* with distance to the cluster center;
- (ii) CO line studies of Williams et al. (1994) show that star-formation activity is more intense in the $H\text{II}$ -region/molecular cloud interface region than in the molecular cloud center.

However, the triggered star-formation scenario is likely not *sequential*. Roman-Zuniga et al. (2008) point out that the relative age differences of the clusters are not consistent with a sequential triggered star formation scenario. They propose that the overall

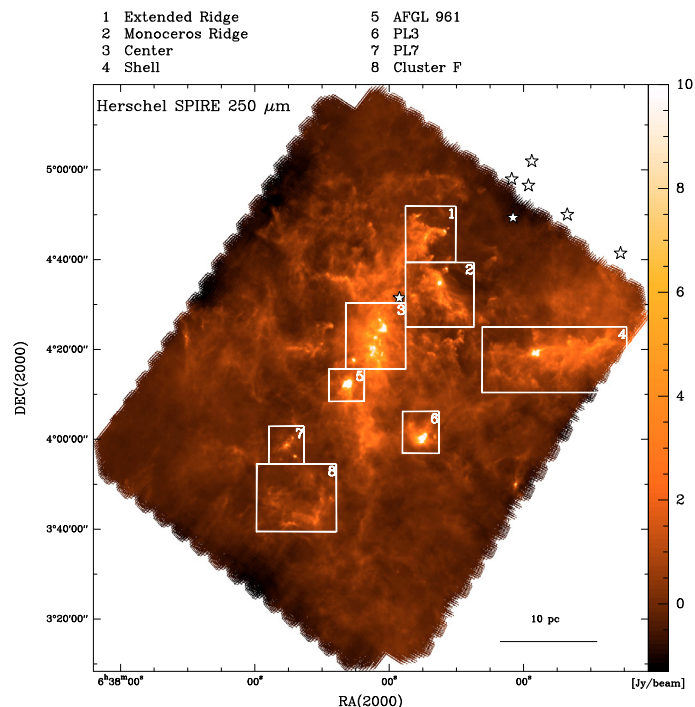


Fig. 2. *Herschel*/SPIRE map at $250\ \mu\text{m}$ of Rosette. Individual regions referred to in the text are numbered and labeled. The stars indicate the seven O-stars (O4 to O9) of NGC 2244.

age sequence of cluster formation could be primordial, possibly resulting from the formation and evolution of the molecular cloud itself. It is thus unclear whether the star-formation activity in Rosette is progressing from the $H\text{II}$ -region interface into the cloud center, or whether it is a global process with a random spread of evolutionary stages and no obvious link between more and less evolved star-forming sites.

2. Observations

The RMC was chosen as a representative source (in terms of mass, star-formation activity etc.) for the HOBYS (*Herschel* imaging survey of OB Young Stellar objects) guaranteed time key program (Motte et al. 2010) on the *Herschel* satellite (Pilbratt et al. 2010), using the SPIRE (Griffin et al. 2010; Swinyard et al. 2010), and PACS (Poglitch et al. 2010) continuum arrays. The SPIRE and PACS data from 70 to $500\ \mu\text{m}$ were obtained on October 20th 2009 in the parallel mode with a scanning speed of $20''/\text{s}$. Two cross-linked coverages of size $1^\circ 45' \times 1^\circ 25'$ were performed, focussing on the southeast corner of the Rosette nebula, i.e. the main part of the molecular cloud (see Fig. 2) The SPIRE data were reduced with HIPE 2.0, using modified versions of the pipeline scripts (for example observations that were taken during the turnaround at the map borders were included). A median baseline and the “naive-mapper” (i.e. a simple averaging algorithm) were applied to the data.

3. Results and analysis

3.1. Three-color image

Figure 1 displays a three-color composite (70 , 160 , and $500\ \mu\text{m}$) image of the RMC, overlaid on a $H\alpha$ image of the region. Blue represents the shortest wavelength ($70\ \mu\text{m}$) and thus the warmest gas phase, green the $160\ \mu\text{m}$ emission, and red the coldest gas phase, traced by $500\ \mu\text{m}$ emission. The $H\text{II}$ -region/molecular

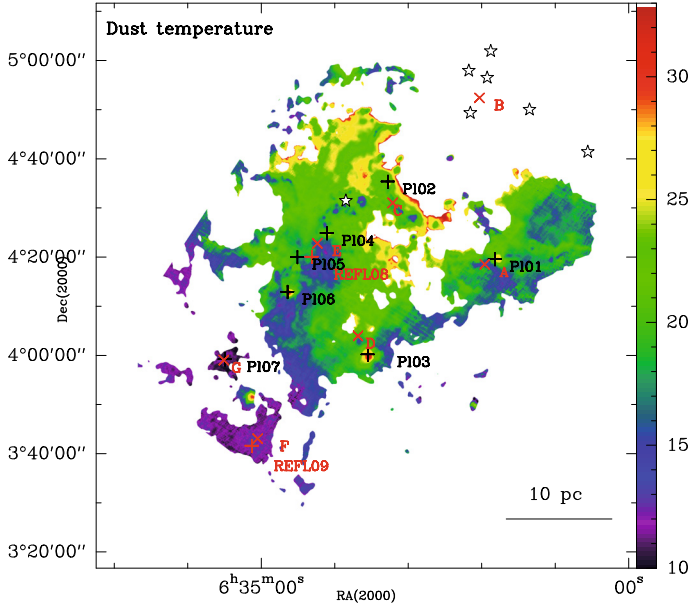


Fig. 3. Dust-temperature map of the Rosette molecular cloud, obtained from simultaneously fitting the five observing wavebands of PACS and SPIRE. The temperature scaling in Kelvin is given on the right. Note that there is probably a zero-point offset in the maps due to the median filter on the scan legs. Only areas that are covered by SPIRE and PACS are shown. Black crosses and label “PL” indicate the position of the clusters identified by Phelps & Lada (1997), red crosses and label “A”, “B” etc. the clusters from Poulton et al. (2008), and label “REFL” the clusters from Roman-Zuniga et al. (2008).

cloud interface, where the UV radiation has the largest impact, is more prominent in blue and shows the most complex and filamentary structure. There, the UV radiation from the NGC 2244 cluster (the 7 O- and 24 B-stars induce a streaming velocity at the ionization front of up to 20 km s^{-1} , Fountain et al. 1979) has erased the low-density gas, leaving only the densest gas as “pillars”. Assuming a cluster age of $2 \times 10^6 \text{ yr}$ (Wang et al. 2009) and a typical expansion velocity of the ionization front of 10 km s^{-1} , this would imply that the radiation penetrates to a depth of $\sim 10 \text{ pc}$. This is indeed approximately the border between the warm and colder gas phase.

Penetrating deeper into the cloud, the cold and dense “molecular ridge” (mostly appearing in pink/red) is less influenced by UV radiation and appears less structured. This does not imply that the gas there has a smoother structure because (i) the lower-density gas still present in this part of the cloud smoothes the distribution; and (ii) resolution effects may play a role. The “coldest” region is found in a remote part of the cloud at 20–30 pc, close to cluster PL7 (see Fig. 2) and beyond.

3.2. Dust temperature and column density

Figure 3 shows the distribution of the dust temperature obtained from a greybody fit to the five observed wavebands at each pixel (all maps were smoothed to the beamsize of the $500 \mu\text{m}$ map, i.e. $\sim 37''$). A dust emissivity index of $\beta = 2$ and a dust opacity of $\kappa = 0.1 * (\nu/1000)^\beta [\text{cm}^2/\text{g}]$ were used. The highest temperatures are found at the H II-region/molecular cloud interface at the Monoceros Ridge and Shell region, indicated by a thin layer of temperatures around 30 K. The temperature then gradually decreases into the molecular cloud down to around 10–15 K in the remote part of the cloud. This is consistent with the dust color

temperatures derived with the IRAS 60/100 μm ratio (Schneider et al. 1998b), which gives 30 K at the H II-region/molecular cloud interface and 26 K in the remote part of the cloud at the position of AFGL961. (Note that the latter values are derived from low-angular resolution IRAS data.)

The temperature gradient indicated by the PACS/SPIRE observations confirms earlier findings by Cox et al. (1990), who showed that 60 and 100 μm IRAS emission is strong in the molecular cloud and nebula region, while the 12 μm emission is prominent in the molecular cloud and inside the H II-region. Dent et al. (2009) detected a decreasing (into the cloud) surface temperature of the clumps due to a decreasing $^{12}\text{CO } 3 \rightarrow 2/1 \rightarrow 0$ line ratio. Not all sites of star formation are correlated with temperature peaks. Clusters A, C, D, E, F, G(=PL7) and PL5 do not appear prominent in the temperature map. In contrast, one strong temperature peak in the remote part of the cloud (between PL7 and F) is not identified as a cluster.

From the column density map (Fig. 5, right), derived from the greybody fit, we calculated the total mass of the complex mapped with *Herschel* to be $\sim 10^5 M_\odot$. The mass and average density of the individual regions is given in Table 1. Interestingly, there is a clear increasing gradient in average density from the H II-region into the molecular cloud. In the “compression” zone of the molecular cloud/H II-region interface (Shell/Extended and Monoceros Ridge), the densities are around $0.5 \times 10^3 \text{ cm}^{-3}$, while the most remote clouds (Cluster F and PL7) have a higher density of $1.8 \times 10^3 \text{ cm}^{-3}$ and $3.9 \times 10^3 \text{ cm}^{-3}$, respectively.

3.3. A closer look at individual regions

Following the notation given in Fig. 2, we show the *Extended Ridge* in Rosette in more detail. Other regions (the *Center* and the *Monoceros Ridge*) can be found as online figures. The *Extended Ridge* represents dense, molecular pillars that are exposed to the ionizing radiation from the NGC 2244 cluster. There are strong temperature and density gradients, visible in the maps of dust temperature, column density, and in the three-color plot shown in Fig. 4. The region of highest column density forms a chain of cold, dense gas clumps, as can be seen in the overlay between 70 μm and 350 μm emission in Fig. 4 where the coldest regions do not appear in 70 μm emission. The masses of these clumps range between 19 and 161 M_\odot , and their average density is typically $1.1 \times 10^4 \text{ cm}^{-3}$ (values determined from the column density map). Though this average density is not low, it is far from the densities of 10^7 cm^{-3} predicted by turbulence models for pillar formation (Gritschneider et al. 2009).

4. Discussion

The prestellar and protostellar population of Rosette observed with *Herschel* was identified with two source extraction techniques that are both based on the principle that emission on large spatial scales is filtered out in order to focus on compact sources. Motte et al. (2010) discuss the core population (prestellar, protostellar, and warm cores on a size scale 0.05–0.3 pc). Di Francesco et al. (2010) present the *clump* distribution (up to 1 pc), which is either starless or associated with YSO.

Figure 1 in Di Francesco et al. (2010) shows the spatial distribution of starless and protostellar clumps. The latter are concentrated in the densest cloud regions, mainly close to the known star clusters, while the starless clumps are more evenly distributed. No correlation between clump type and distance to the OB cluster is observed that may suggest an age-effect.

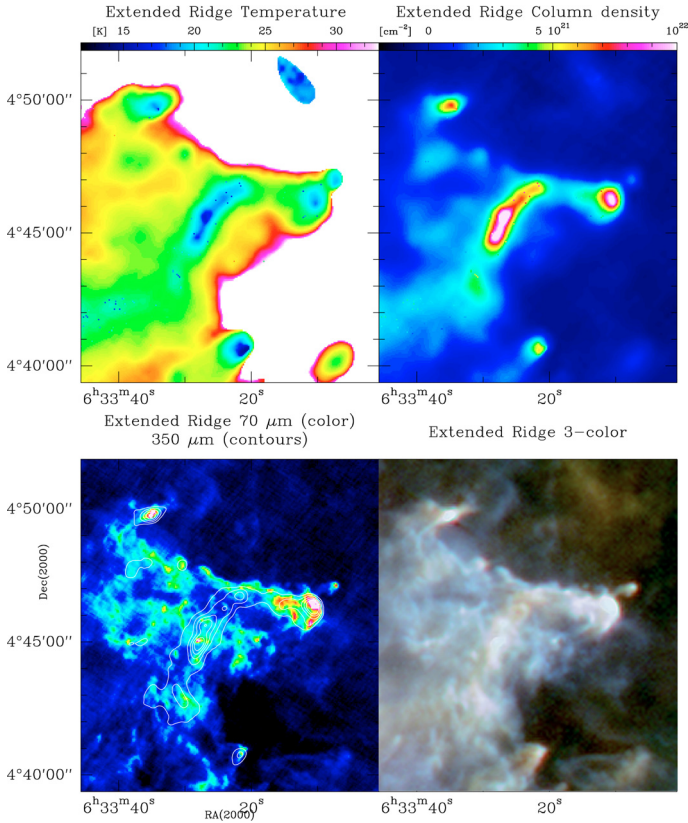


Fig. 4. Zoom into the *Extended Ridge* region. *Upper left*: dust temperature, *upper right*: column density, *lower left*: overlay 70 μm and 350 μm , *lower right*: three-color image (70 μm = blue, 160 μm = green, 250 μm = red). Note that here we used the 250 μm data for the red band.

In Fig. 5 in Motte et al. (2010) the spatial distribution of the most massive dense cores is shown and in our Table 1 the statistics of these sources with regard to the different regions is summarized. We adopt the classification for prestellar cores to evolved YSO defined in Motte et al. (2010) and compute the relative numbers of young vs. evolved sources in each region (last column in Table 1). The resulting sequence *may* indicate that there is an age-gradient across the RMC with the PL7 cluster being the youngest, in the remote part of the cloud, and the Monoceros Ridge and Shell Region, close to the H II-region, being the most evolved. An independent confirmation of the youth of cluster PL7 is given in Hennemann et al. (2010) in their protostellar envelope mass vs. bolometric luminosity diagram. Note that Roman-Zuniga et al. (2008) also detected an increasing fraction of young stars with increasing distance to the NGC 2244 cluster center and Balog et al. (2007) found that the Class II sources are concentrated at the center of NGC 2244, while the Class I sources are located further away from the cluster. On the other hand, cluster PL3 does not fit this scenario well, because it seems to be a more evolved region, but is located in the more remote part of the cloud. A tentative explanation may be that because it is more exposed to UV radiation and thus less shielded by denser gas, (like the Center and remote region) its evolution might have been accelerated by the radiative impact. However, we emphasize that there are not enough sources analyzed so far to draw a firm conclusion. A more detailed analysis with a larger sample and significant statistics is required, which is planned for the future.

Table 1. Age-sequence of the sources found in Rosette.

Region	d [pc]	$\langle n \rangle$ [10^3 cm^{-3}]	M [M_{\odot}]	Young/ evolved
7 PL7	35	3.9	2080	3/0
6 PL3	27	1.5	1650	1/3
5 AFGL961	25	9.5	792	4/1
3 Center	20	0.6	22 250	9/4
1+2 Ext. + Mon. Ridge	10	0.6	4280	6/3
4 Shell	10	0.4	11 780	1/2

Notes. The regions are ordered with decreasing distance (d) from the center of NGC 2244 (for simplicity we take as “center” the position of cluster B in Fig. 3). The average density ($\langle n \rangle$) and mass (M) were derived from the column density by determining the area of each region and assuming the same extent of the cloud along the line of sight. The last column gives the number of sources (young vs. evolved).

Acknowledgements. SPIRE has been developed by a consortium of institutes led by Cardiff University (UK) and including Univ. Lethbridge (Canada); NAOC (China); CEA, LAM (France); IFSI, Univ. Padua (Italy); IAC (Spain); Stockholm Observatory (Sweden); Imperial College London, RAL, UCL-MSSL, UKATC, Univ. Sussex (UK); and Caltech, JPL, NHSC, Univ. Colorado (USA). This development has been supported by national funding agencies: CSA (Canada); NAOC (China); CEA, CNES, CNRS (France); ASI (Italy); MCINN (Spain); SNSB (Sweden); STFC (UK); and NASA (USA). PACS has been developed by a consortium of institutes led by MPE (Germany) and including UVIE (Austria); KU Leuven, CSL, IMEC (Belgium); CEA, LAM (France); MPIA (Germany); INAF-IFSI/OAA/OAP/OAT, LENS, SISSA (Italy); IAC (Spain). This development has been supported by the funding agencies BMVIT (Austria), ESA-PRODEX (Belgium), CEA/CNES (France), DLR (Germany), ASI/INAF (Italy), and CICYT/MCYT (Spain). Part of this work was supported by the ANR (*Agence Nationale pour la Recherche*) project “PROBeS”, number ANR-08-BLAN-0241. The figures were prepared using GILDAS¹ and with the help of the ESA/ESO/NASA Photoshop FITS Liberator. We thank the referee, Marc Pound, for his critical comments.

References

- Balog, Z., Muzerolle, J., Rieke, G. H., et al. 2007, *ApJ*, 660, 1532
 Cox, P., Deharveng, L., & Leene, A. 1990, *A&A*, 230, 181
 Dent, W. R. F., Hovey, G. J., Dewdney, P. E., et al. 2009, *MNRAS*, 395, 1805
 Deharveng, L., Zavagno, A., & Caplan, J. 2005, *A&A*, 433, 565
 Di Francesco, J. 2010, *A&A*, 518, L91
 Elmegreen, B., & Lada, C. 1977, *ApJ*, 214, 725
 Fountain, W. F., Gary, G. A., & Odell, C. R. 1979, *ApJ*, 229, 971
 Griffin, M. J. 2010, *A&A*, 518, L3
 Gritschneider, M., Naab, T., Walch, S., et al. 2009, *ApJ*, 694, L26
 Heyer, M. H., Williams, J. P., & Brunt, C. M. 2006, *ApJ*, 643, 956
 Lefloch, B., & Lazareff, B. 1994, *A&A*, 289, 559
 Li, J. Z., & Smith, M. D. 2005, *ApJ*, 620, 816
 Motte, F. 2010, *A&A*, 518, L77
 Patel, N. A., Xie, T., & Goldsmith, P. F. 1993, *ApJ*, 413, 593
 Pilbratt, G. L. 2010, *A&A*, 518, L1
 Phelps, R. L., & Lada E. A. 1997, *ApJ*, 477, 176
 Poglitsch, A. 2010, *A&A*, 518, L2
 Poulton, C., Robitaille, T. P., Greaves, J. S., et al. 2008, *MNRAS*, 384, 1249
 Roman-Zuniga, C. G., Elston, R., Ferreira, B., & Lada, E. 2008, *ApJ*, 672, 861
 Schneider, N., Stutzki, J., Winnewisser, G., et al. 1998a, *A&A*, 335, 1049
 Schneider, N., Stutzki, J., Winnewisser, G., et al. 1998b, *A&A*, 338, 262
 Schneider, N., Bontemps, S., et al. 2010, *A&A*, submitted [arXiv:1001.2453]
 Schneps, M. H., Ho, P. T. P., & Barrett, A. H. 1980, *ApJ*, 240, 84
 Swinyard, B. M. 2010, *A&A*, 518, L4
 Wang, J., Feigelson, E. D., Townsley, L. K., et al. 2009, *ApJ*, 696, 47
 White, G., Lefloch, B., Fridlund, C. V. M., et al. 1997, *A&A*, 323, 931
 Williams, J. P., de Geus, E. J., & Blitz, L. 1994, *ApJ*, 428, 693

¹ <http://iram.fr/IRAMFR/GILDAS>

-
- ¹ Laboratoire AIM, CEA/DSM – INSU/CNRS – Université Paris Diderot, IRFU/Sap CEA-Saclay, 91191 Gif-sur-Yvette, France
e-mail: nschneid@cea.fr
- ² Laboratoire d’Astrophysique de Bordeaux, CNRS/INSU – Université de Bordeaux, BP 89, 33271 Floirac Cedex, France
- ³ National Research Council of Canada, Herzberg Institute of Astrophysics, University of Victoria, Department of Physics and Astronomy, Victoria, Canada
- ⁴ Laboratoire d’Astrophysique de Marseille, CNRS/INSU – Université de Provence, 13388 Marseille Cedex 13, France
- ⁵ IAS, Université Paris-Sud, 91435 Orsay, France
- ⁶ CESR & UMR 5187 du CNRS/Université de Toulouse, BP 4346, 31028 Toulouse Cedex 4, France
- ⁷ IRAM, 300 rue de la Piscine, Domaine Universitaire, 38406 Saint Martin d’Hères, France
- ⁸ INAF-IFSI, Fosso del Cavaliere 100, 00133 Roma, Italy
- ⁹ Cardiff University School of Physics and Astronomy, UK
- ¹⁰ National Astronomical Observatories, Chinese Academy of Sciences, Beijing 100012, PR China
- ¹¹ Space Science and Technology Department, Rutherford Appleton Laboratory, Didcot, Oxon OX11 0QX, UK
- ¹² Herschel Science Centre, ESAC, ESA, PO Box 78, Villanueva de la Cañada, 28691 Madrid, Spain
- ¹³ CITA & Dep. of Astronomy and Astrophysics, University of Toronto, Toronto, Canada
- ¹⁴ Department of Astronomy, Stockholm University, AlbaNova University Center, Roslagstullsbacken 21, 10691 Stockholm, Sweden
- ¹⁵ INAF-IASF, Sez. di Roma, via Fosso del Cavaliere 100, 00133 Roma, Italy
- ¹⁶ UPMC Université de Paris 06, UMR7095, IAP, 75014 Paris, France
- ¹⁷ Astronomy Technology Centre, Royal Observatory Edinburgh, Blackford Hill, EH9 3HJ, UK
- ¹⁸ ESO, Karl Schwarzschild Str. 2, 85748, Garching, Germany
- ¹⁹ Department of Physics and Astronomy, McMaster University, Hamilton, Canada
- ²⁰ SUPA, Institute for Astronomy, Edinburgh University, Blackford Hill, Edinburgh EH9 3HJ, UK
- ²¹ Department of Physics & Astronomy, The Open University, Milton Keynes MK7 6AA, UK

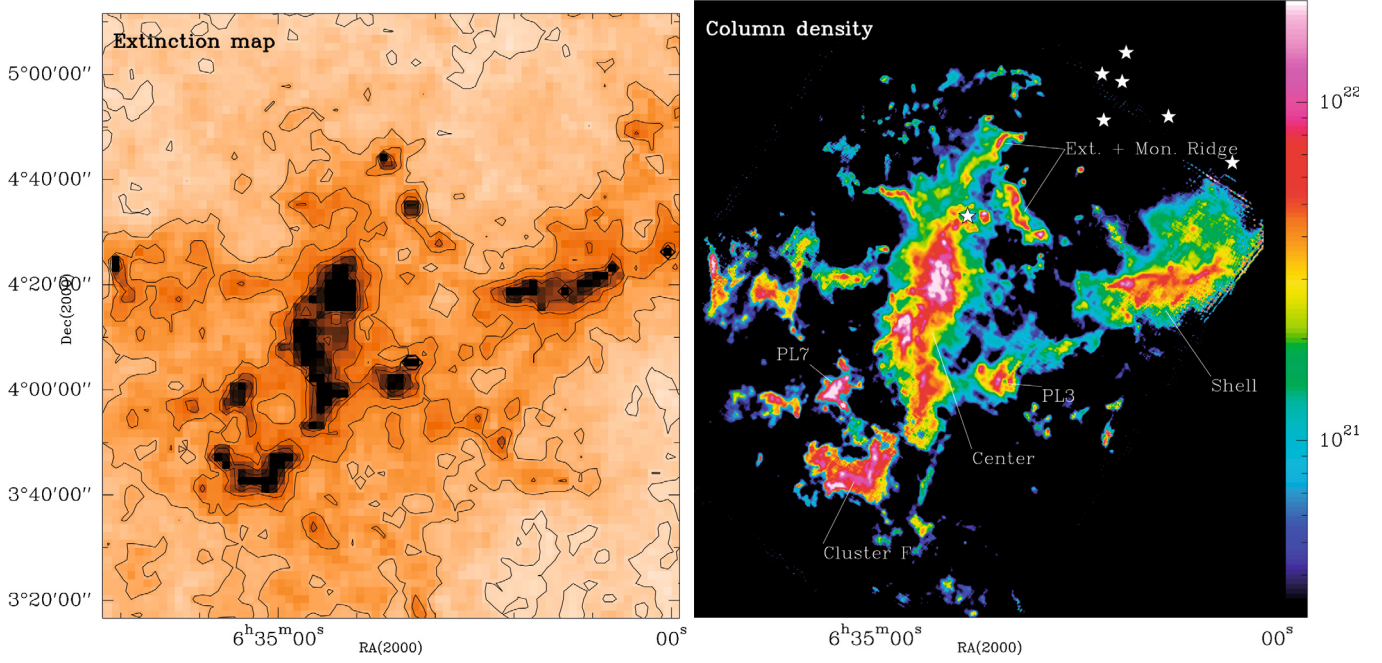


Fig. 5. *Left:* extinction map of the RMC, derived from stellar reddening of background stars in *JHK*, using the 2MASS database, and a pixel size of 1.3' (Bontemps, priv. comm.; Schneider, et al. 2010). Contour levels increase from $A_V = 2^m$ to 14^m in steps of 2^m . *Right:* molecular hydrogen column density [cm^{-2}] in logarithmic scaling determined from the same greybody fit that was used for the temperature. The regions referred to in Table 1 are indicated.

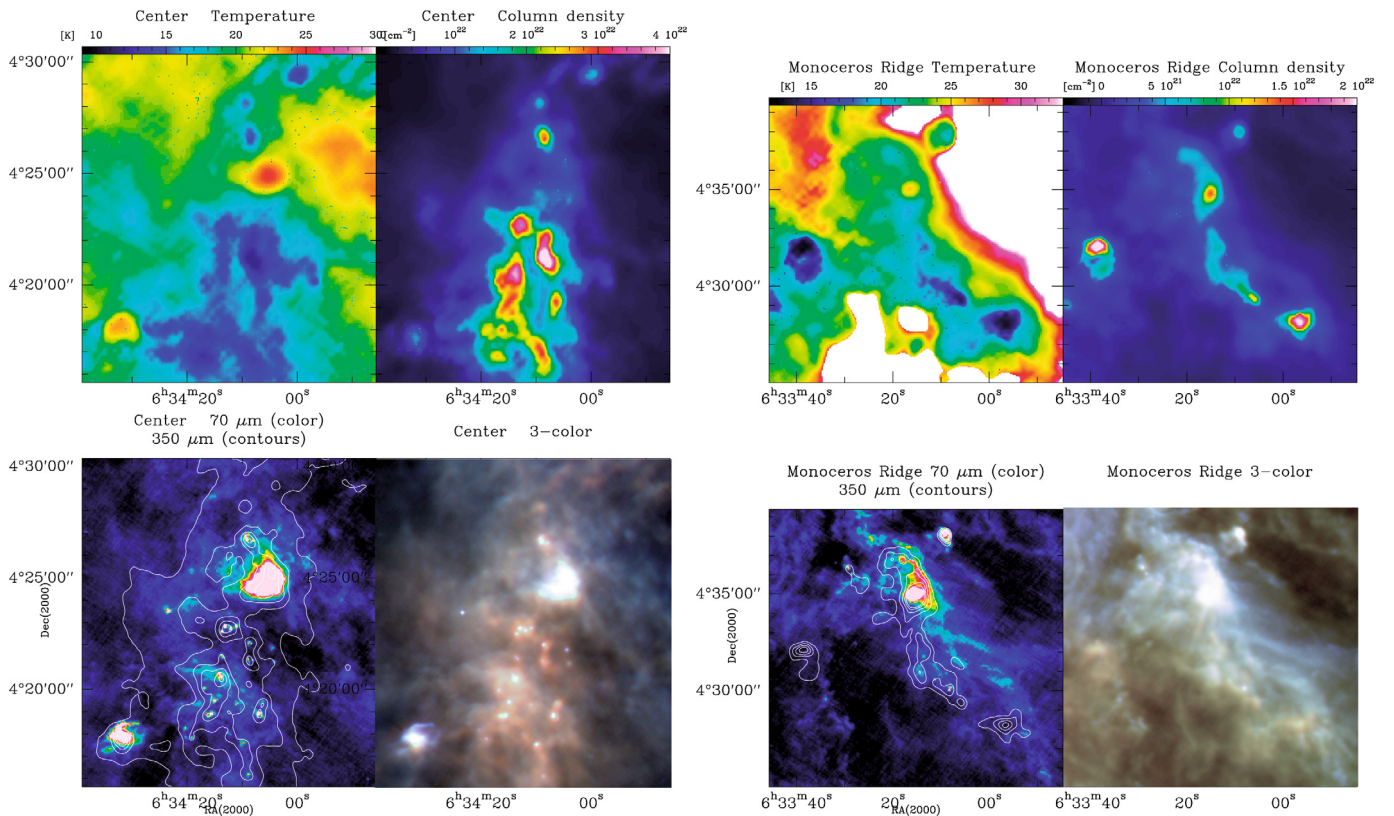


Fig. 6. Zoom into the *Center* (left) and *Monoceros Ridge* (right) regions, similar to the Extended Ridge presented in Fig. 4. *Upper row:* dust temperature, and column density plots of each region, respectively. *Lower row:* overlay 70 μm and 350 μm , and three-color image (70, 160, 250 μm) of each region, respectively.